Zuschriften

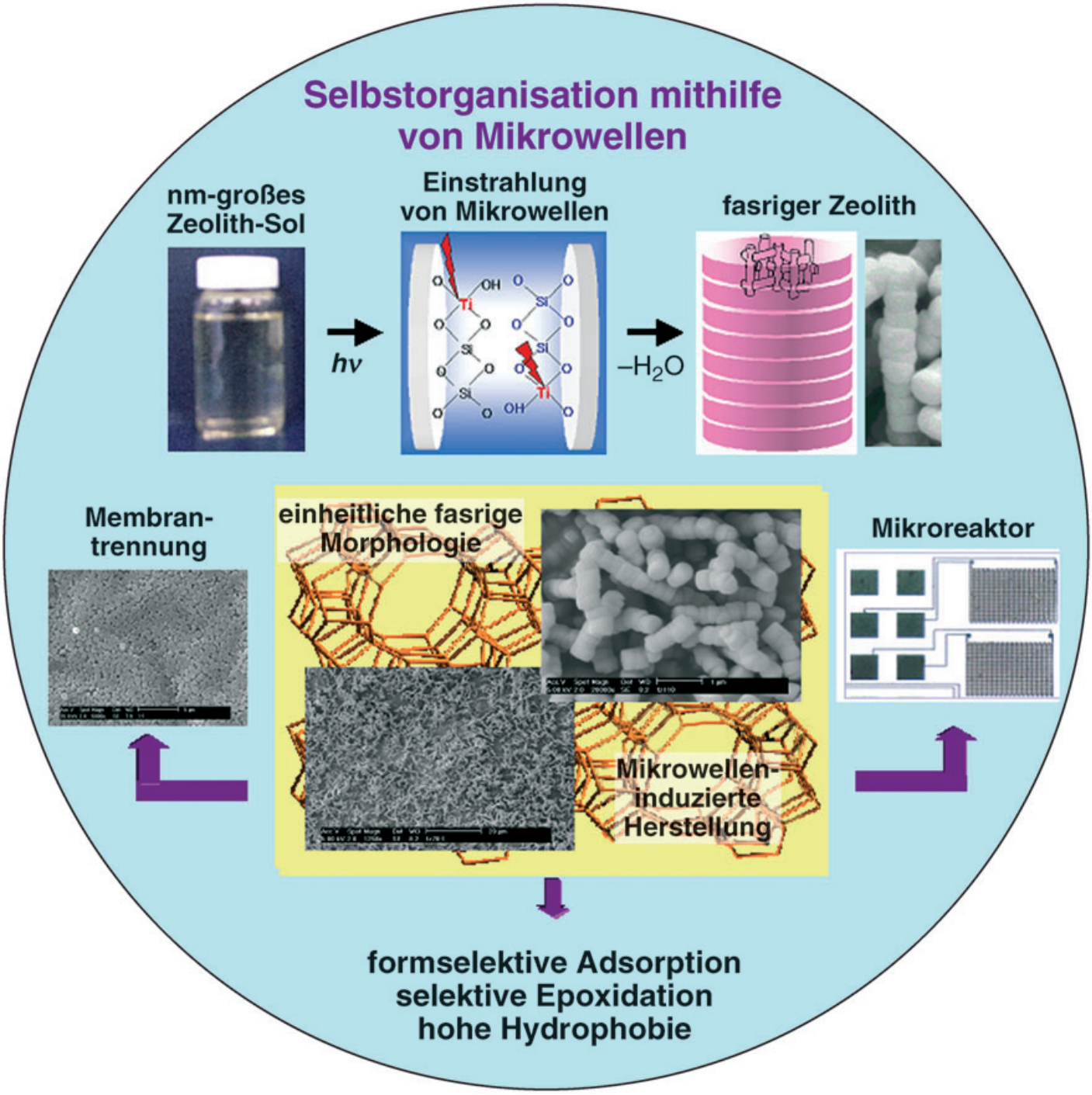

Metallhaltige Zeolithe, die unter Einstrahlung von Mikrowellen hergestellt wurden, bilden eine fasrige Morphologie. Die Materialien zeigen eine bessere formselektive Adsorption von Xylolisomeren und kommen für Anwendungen in Mikroreaktoren und in der Trenntechnik infrage. Einzelheiten finden Sie in der Zuschrift von J.-S. Chang, S.-E. Park et al. auf den folgenden Seiten.

DOI: 10.1002/ange.200461403

Zeolite Synthesis

Microwave Fabrication of MFI Zeolite Crystals with a Fibrous Morphology and Their Applications**

Young Kyu Hwang, Jong-San Chang, Sang-Eon Park,* Dae Sung Kim, Young-Uk Kwon, Sung Hwa Jhung, Jin-Soo Hwang, and Min Seok Park*

Zeolite molecular sieves are good candidates for designed microscopically and nanoscopically engineered materials due to their well-defined pore structures.[1,2] Among them, silicalites, zeolites having the MFI framework topology, have been studied extensively with regards to the selective separation of hydrocarbons[3] and the development of electrode materials,[4] membranes,[5] and catalysts.[6] Because many emerging applications of porous materials require precise control of crystal size, shape, and orientation,[7,8] the development of new synthesis strategies is increasingly important. For example, the properties of spherical mesoporous silica particles with a narrow particle size distribution as a material for column chromatography are superior to those of curved hexagonal rods with the same structure.[7]

Recently, it has been reported that the microwave synthesis method could provide an efficient way to control particle size distribution,[9] phase selectivity,[10] and macroscopic morphology[11] in the synthesis of porous materials as well as result in fast crystallization.[12] However, to our knowledge, there are few reports of microwave techniques being utilized to control the morphology of porous materials.[11,13] Here, we report on new applications of the microwave method for the fabrication of MFI-type zeolite crystals incorporating Ti and other metal species. By using the method, we prepared fibrous MFI zeolites that exhibited useful physicochemical properties due to their self-stacking.

Pure and metal-incorporated MFI crystals were synthesized by microwave-heating precursor solutions at 438 K. These samples will be denoted as M-MFI-MW, where M stands for the incorporated metal (Ti, Fe, Zr, and Sn) and MW for the microwave conditions; metal-free MFI from a microwave reaction will be denoted as Si-MFI-MW.

The powder X-ray diffraction (XRD) patterns of Ti-MFI-MW samples show the characteristic peaks for the MFI structure without any impurities. The IR spectra of the calcined Ti-MFI-MW samples exhibit an absorption band at 960 cm^{-1} for the stretching mode of a [SiO_4] unit bonded to a Ti^{4+} ion (O_3SiOTi). UV/Vis diffuse reflectance spectra, collected in vacuo after evacuation ($\leq 10^{-5}$ torr) at 627 K, revealed a strong peak around 210–240 nm, assignable to the ligand-to-metal charge-transfer absorption band from the oxygen to tetrahedral titanium(IV) atom in the zeolite framework.[14] The Ti-MFI-CH from the hydrothermal syntheses also showed practically the same XRD and IR data, indicating that the difference in the synthesis methods did not influence the identity of the final products.

However, we observed that the microwave synthesis induces a dramatic change in the morphology depending on the composition. Si-MFI-MW and Ti-MFI-CH show the characteristic pucklike crystals of submicrometer sizes with well-developed large (010) faces (Figure 1a and b). The aggregated morphology of individual particles appears to be attributed to superfast crystallization (Figure 1b).[9] The microwave reactions of incorporated metal systems produced similar primary crystals, but this time the crystals are all

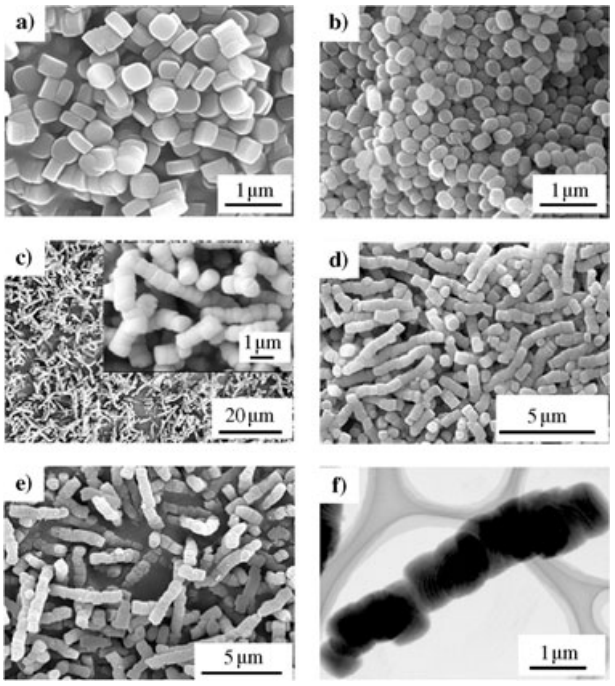

Figure 1. SEM images of a) Si-MFI-MW, b) Ti-MFI-CH (Si/Ti = 70), c) Ti-MFI-MW (Si/Ti = 120), d) Ti-MFI-MW (Si/Ti = 70), and e) Sn-MFI-MW, and f) TEM image of Sn-MFI-MW. Inset is a large-scale image of (c).

[*] Dr. Y. K. Hwang, Dr. J.-S. Chang, Dr. D. S. Kim, Dr. S. H. Jhung, Dr. J.-S. Hwang, Dr. M. S. Park
Research Center for Nanocatalysis
Korea Research Institute of Chemical Technology (KRICT)
P.O. Box 107, Yusung, Taejon 305-600 (Korea)
Fax: (+82) 42-860-7676
E-mail: jschang@krict.re.kr
Prof. S.-E. Park
Department of Chemistry, Inha University
Incheon 402-751 (Korea)
Fax: (+82) 32-874-7674
E-mail: separk@inha.ac.kr
Prof. Y.-U. Kwon
Department of Chemistry and BK-21
School of Molecular Science, Sungkyunkwan University
Suwon 440-746 (Korea)

[**] This work was supported by the Korean Ministry of Science and Technology through the National Science Programs for Key Nanotechnology and Institutional Research Program. The authors thank especially Prof. J. M. Kim for helpful collaboration, Dr. C. H. Xue and T. H. Jin for experimental assistance, and Dr. J. S. Yoo and P. M. Forster for useful discussions.

Supporting information for this article is available on the WWW under http://www.angewandte.org or from the author.

stacked on top of one another along their [010] direction to form a wormlike or fibrous morphology (Figure 1c–f). This stacking is sufficiently robust that it is not destroyed by sonication for 1 h or more, indicating that this morphology is not a result of simple aggregation but of strong chemical bonds between the crystals. This fibrous morphology persists as long as there is incorporated Ti and its concentration is kept in the range of Si/Ti = 70–230. When the concentration of Ti is increased (Si/Ti ≤ 50), the product is composed of isolated ellipsoidal crystals (not shown). This is probably because the high concentration of Ti interferes with the mechanism of crystal growth, and the lack of flat surfaces does not allow crystal stacking. The crystals with other incorporated metals (Fe, Zr, Sn) also show the fibrous morphology, and we show the images of Sn-MFI-MW in Figure 1e and f.

We also have monitored the reaction progress in the Ti-MFI-MW system by XRD and scanning electron microscopy (SEM). The XRD patterns show that the crystals are starting to grow out of embryos after about 10 min, grow rapidly during the next 30 min, and reach the full crystallization at about 60 min. The SEM images show that the stacking of crystals begins at 20 min and culminates after 60 min. These observations suggest that the fibrous morphology is achieved through interactions between already present crystals (see the Supporting Information).

Although it is not clear how the incorporated metals induce the stacking of crystals under the microwave conditions, it appears to be related with the magnitude of the local dipole moment of the M–O bonds. Electrically insulating materials absorb microwave energy through the oscillation of dipoles, and the magnitude of absorption increases with an increase in the dipole moment. The magnitude of the dipole moment is determined mainly by the difference in the electronegativities ($\Delta\chi$) of the two bonded atoms. Therefore, the Ti–O bond ($\Delta\chi = 2.18$ according to the Allred–Rochow scheme)[15] is a better microwave absorber than the Si–O bond ($\Delta\chi = 1.76$). The Ti–O bonds on the surfaces are strongly activated by microwave absorption and can undergo condensation reactions to form Ti-O-Ti and/or Ti-O-Si bonds between crystals. The same explanation applies to the Fe-MFI-MW and Zr-MFI-MW zeolites because of the large $\Delta\chi$ values for Fe–O and Zr–O bonds. In the case of Sn-MFI-MW, the $\Delta\chi$ value of the Sn–O bond (1.78) is rather small, close to that of Si–O bond. However, because Sn is a large atom, the valence electron density of the Sn–O bond is shifted to the O side, making this bond more polar than would be estimated by the $\Delta\xi$ value alone. In other words, the homopolar contribution to the dipole moment[16] and the above explanation of microwave absorption by polar bonds can be applied to the Sn-MFI-MW case. Further work is needed to fully understand the role of the incorporated metals in the stacking of crystals under microwave conditions.

The concentration of the reagent also influences the stacking behavior of crystals. When the concentration is too low ($H_2O/SiO_2 = 50$ and 100), the crystals become larger than those mentioned above ($H_2O/SiO_2 = 22$) and the stacking occurs to a much lesser extent. Probably, the large crystal sizes and the dilute conditions provide fewer chances for the crystals to meet with the correct relative orientation for stacking. When the concentration is too high ($H_2O/SiO_2 = 10$), the product is composed of granules of much smaller sizes because the reaction occurs too quickly for the crystals to attain the pucklike morphology, and the lack of large and flat surfaces prohibits the crystal stacking.

The fibrous morphology of Ti-MFI-MW crystals leads to several unique properties that may be advantageous for applications. To show this, we chose a fibrous Ti-MFI-MW synthesized from a Si/Ti = 70 solution and compared its properties with those of nonfibrous MFI zeolites such as Si-MFI-MW, Ti-MFI-CH, and Ti-MFI-MW (hereafter, NF-Ti-MFI-MW) synthesized from a solution with $H_2O/SiO_2 = 100$. The packing density of fibrous Ti-MFI-MW powder is 1.9 times lower than that of the Si-MFI-MW and Ti-MFI-CH powders. However, the BET surface areas and micropore volumes from N_2-adsorption experiments (Table 1) show that all three Ti-MFIs (Ti-MFI-MW, Ti-MFI-CH, and NF-Ti-MFI-MW) have comparable pore characteristics, suggesting that the crystal stacking hardly affects the intracrystalline pore structure and that the reduced density of Ti-MFI-MW is a result of the fibrous morphology. The hydrophobicity index data from the adsorption mass ratio of toluene and water show that the hydrophobicity of fibrous Ti-MFI-MW is 36% higher than that of Ti-MFI-CH (Supporting Information). It can be rationalized in terms of the consumption of terminal hydroxyl groups by stacking crystals in Ti-MFI-MW. According to IR spectra of Ti-MFI-MW dehydrated at 673 K under vacuum, the intensity of surface hydroxyl band (ca. 3740 cm^{-1}) of the Ti-MFI-MW is much smaller than those of

Table 1: Physicochemical and catalytic properties of Ti-MFI zeolites according to the morphology and preparation method.

Catalyst[a]	S_{BET} [$m^2 g^{-1}$]	Pore volume [$mL g^{-1}$]	Hydrophob. index[b]	Reaction time [h]	Styrene epoxidation[c] Conv. [%][d]	Sel. [%][e]
Ti-MFI-MW (fibrous)	423	0.21	8.2	4	55.6	63.1
				8	70.5	65.2
NF-Ti-MFI-MW (nonfibrous)	432	0.22	6.3	4	39.5	54.5
				8	48.7	51.9
Ti-MFI-CH (nonfibrous)	453	0.25	6.0	4	39.5	52.5
				8	48.0	44.2

[a] Ti-MFI-MW (fibrous): prepared by microwave irradiation for 60 min with a H_2O/SiO_2 ratio of 22; NF-Ti-MFI-MW (nonfibrous): prepared by microwave irradiation for 60 min with a H_2O/SiO_2 ratio of 100; Ti-MFI-CH (nonfibrous): prepared by the conventional hydrothermal method at 438 K for 24 h in a Si/Ti ratio of 70. [b] The hydrophobicity index was calculated from the amount of adsorbed water and toluene. [c] Reaction conditions: 343 K, 5 mL styrene, 1.3 mL H_2O_2 (30%), 18 mL acetone (solvent), 0.35 g catalyst. [d] (Styrene conversion/maximum expected conversion) × 100. [e] Other products: benzaldehyde and phenylacetaldehyde.

Ti-MFI-CH and even NF-Ti-MFI-MW. (Supporting Information). The enhanced surface hydrophobicity affects the catalytic properties of Ti-MFI-MW. As summarized in Table 1, Ti-MFI-MW is more reactive and selective than nonfibrous Ti-MFI-CH and NF-Ti-MFI-MW for the epoxidation of styrene with H_2O_2 to produce styrene oxide. Although the fibrous structure of Ti-MFI-MW may limit the diffusion of reactants and products, this drawback is more than offset by the positive effect of the increased hydrophobicity for this reaction.[17]

Even more importantly, the fibrous Ti-MFI-MW zeolite presents significantly enhanced shape selectivity in adsorption. Figure 2 shows the temperature-programmed desorption

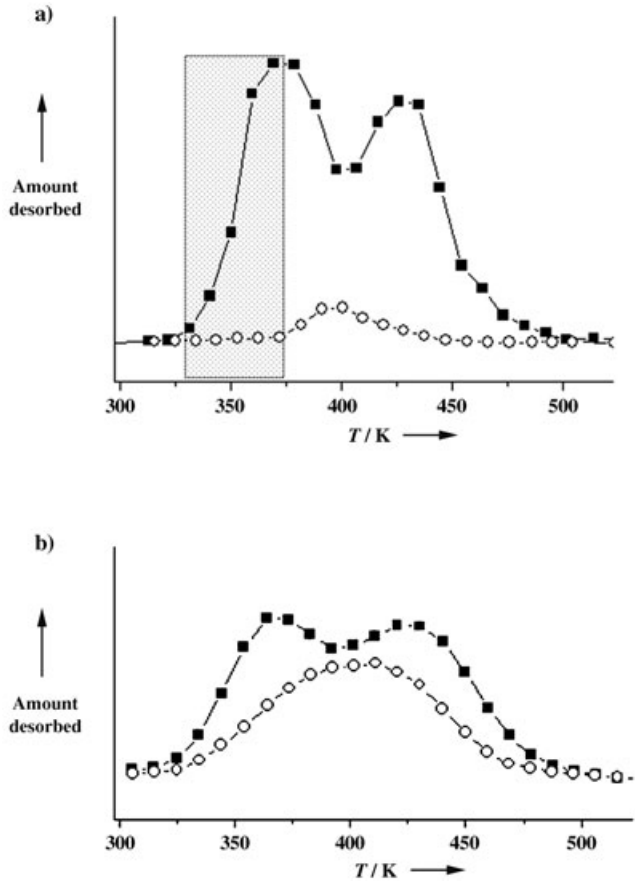

Figure 2. Xylene TPD profiles of a) fibrous Ti-MFI-MW and b) nonfibrous Ti-MFI-CH after vapor-phase competitive adsorption of an equimolar mixture of *p*-xylene (■) and *o*-xylene (○) at 323 K. Adsorbent weight: 0. 25 g; carrier gas: nitrogen (flow rate = 30 mL min^{-1}); ramp rate = 5 K min^{-1}; mL xylenes per gram of adsorbent = 0.168 for plot a and 0.175 for plot b.

(TPD) profiles of xylene isomers after vapor-phase adsorption of an equimolar mixture of *p*-xylene and *o*-xylene over Ti-MFI-MW and Ti-MFI-CH at 323 K.[3,8] The xylene TPD patterns are similar over the two adsorbents, that is, two peaks for *p*-xylene and one peak for *o*-xylene, while the fibrous Ti-MFI-MW reveals a remarkably enhanced adsorption selectivity to *p*-xylene (*p*-xylene/*o*-xylene = 10.7), which is 6.7 times higher than that of the nonfibrous Ti-MFI-CH. Moreover, it is notable that Ti-MFI-MW selectively desorbs only *p*-xylene in the low-temperature range 323–373 K (shaded area of Figure 2 a), implying that this material can be applied in producing highly pure *p*-xylene from a xylene mixture when combined with temperature swing desorption. The preferential adsorption of *p*-xylene (*p*-xylene/*o*-xylene = 9.9) in the fibrous Ti-MFI-MW has also been confirmed in competitive liquid-phase adsorption of a *p*-xylene/*o*-xylene mixture at 293 K (see the Supporting Information).

The MFI structure has three different sites for adsorption: straight and sinusoidal channels along the [010] and [100] directions, respectively, and their intersections. The diffusivity in the straight channel is reportedly much higher than in the sinusoidal channel.[18] Because of the crystal stacking along the [010] direction, the straight channels of Ti-MFI-MW are longer and their openings are much fewer than those of the nonfibrous Ti-MFI-CH crystals. Therefore, the difference between the diffusivities of *p*- and *o*-xylene would be amplified, resulting in the enhanced adsorption selectivity of Ti-MFI-MW. Further work is needed to fully understand the present adsorption behaviors.

In summary, we have demonstrated that the coupled effect of metal incorporation at a suitable concentration level and microwave irradiation during the synthesis of MFI zeolites produces fibrous MFI crystals. This effect appears to be related to the dipole moment strength of the surface M–O bonds. The fibrous Ti-MFI-MW zeolites show several interesting properties such as lower packing density, higher hydrophobicity, enhanced catalytic properties, and higher shape-selectivity in adsorption as compared to nonfibrous MFI zeolites.

Experimental Section

Ti-MFI-MW and Fe-MFI-MW were synthesized at 438 K for 60 min under microwave (MW) irradiation at 600 W. Tetraethyl orthosilicate (TEOS, Aldrich, 98%), tetrapropyl orthotitanate (TPOT, Aldrich, 96%) and tetrapropylammonium hydroxide (TPAOH, Aldrich, 25%) were used. The molar composition of the reaction mixture was 1 TEOS:0.2 TPAOH:0–0.05 TPOT or 0–0.05 $FeCl_3$:1 isopropyl alcohol:22.2 H_2O. The precursor gel of 30–60 g was loaded in a 100-mL Teflon autoclave, which was sealed and placed in a microwave oven (Mars-5, CEM). Ti-MFI-CH was prepared under conventional hydrothermal conditions at 438 K for 24 h with the same precursor-gel composition as Ti-MFI-MW. Sn- and Zr-MFI zeolites were synthesized with the same precursor compositions as Ti-MFI-MW at 438 K except for the modification of metal alkoxides using acetylacetone as a chelating agent to reduce the rate of alkoxide hydrolysis. Further details are given in Supporting Information.

Vapor-phase adsorption and TPD measurements of xylene isomers were conducted in a plug-flow glass reactor with an internal diameter of 6 mm at 323 K. The xylene mixture that passed through the reactor was analyzed using an on-line gas chromatograph (Donam model DS-6200) that was equipped with a capillary column (Bentone-34) and a flame ionization detector. TPD profiles of the adsorbed xylenes were obtained by temperature-programmed heating (ramp rate: 5 K min^{-1}) from 323 K to 573 K after sufficient desorption of physisorbed xylenes at 323 K. Detailed methods for the adsorption and TPD analysis of xylene isomers are described in the Supporting Information.

Received: July 23, 2004
Published online: November 11, 2004

Keywords: crystal growth · microporous materials · zeolites

[1] a) G. A. Ozin, *Adv. Mater.* **1992**, *4*, 612; b) T. Bein, *Chem. Mater.* **1996**, *8*, 1636.
[2] M. E. Davis, *Nature* **2002**, *417*, 813.
[3] a) W. Yuan, Y. S. Lin, W. Yang, *J. Am. Chem. Soc.* **2004**, *126*, 4776; b) .S. Li, C. Demmelmaier, M. Itkis, Z. Liu, R. C. Haddon, Y. Yan, *Chem. Mater.* **2003**, *15*, 2687.
[4] S. Li, X. Wang, D. Beving, Z. Chen, Y. Yan, *J. Am. Chem. Soc.* **2004**, *126*, 4122.
[5] G. Xomeritakis, Z. Lai, M. Tsapatsis, *Ind. Eng. Chem. Res.* **2001**, *40*, 544.
[6] a) B. Notari, *Adv. Catal.* **1996**, *41*, 253; b) V. Ramaswamy, B. Tripathi, D. Srinivas, A. V. Ramaswamy, R. Cattaneo, R. Prins, *J. Catal.* **2001**, *200*, 250.
[7] C. Thoelen, J. Paul, I. F. J. Vankelecom, P. A. Jacobs, *Tetrahedron: Asymmetry* **2000**, *11*, 4819.
[8] Z. Lai, G. Bonilla, S. Diaz, J. G. Nery, K. Sujaoti, M. A. Amat, E. Kokkoli, O. Terasaki, R. W. Thompson, M. Tsapatsis, D. G. Vlachos, *Science* **2003**, *300*, 456.
[9] a) S. Komarneni, R. Roy, Q. H. Li, *Mater. Res. Bull.* **1992**, *27*, 1393; b) C. S. Cundy, *Collect. Czech. Chem. Commun.* **1998**, *63*, 1699; c) C. Gabriel, S. Gabriel, E. H. Grant, B. S. J. Halstead, D. M. P. Mingos, *Chem. Soc. Rev.* **1998**, *27*, 213; d) S.-E. Park, D. S. Kim, J.-S. Chang, W. Y. Kim, *Catal. Today* **1998**, *44*, 301; e) X. Xu, W. Yang, J. Liu, L. Lin, *Adv. Mater.* **2000**, *12*, 195; f) D. P. Serrano, M. A. Uguina, R. Sanz, E. Castillo, A. Rodriguez, P. Sanchez, *Microporous Mesoporous Mater.* **2004**, *69*, 197; g) C. S. Cundy, J. O. Forrest, *Microporous Mesoporous Mater.* **2004**, *72*, 67.
[10] a) S. H. Jhung, J.-S. Chang, J.-S. Hwang, S.-E. Park, *Microporous Mesoporous Mater.* **2003**, *64*, 33; b) S.-E. Park, J.-S. Chang, Y. K. Hwang, S. H. Jhung, D. S. Kim, J. S. Hwang, J.-S. Hwang, *Catal. Surv. Asia* **2004**, *8*, 91.
[11] a) S. H. Jhung, J.-S. Chang, Y. K. Hwang, S.-E. Park, *J. Mater. Chem.* **2004**, *14*, 280; b) Y. K. Hwang, J.-S. Chang, Y.-U. Kwon, S.-E. Park, *Microporous Mesoporous Mater.* **2004**, *68*, 280; c) J.-C. Lin, J. T. Dipre, M. Z. Yates, *Langmuir* **2004**, *20*, 1039.
[12] a) B. L. Newalkar, S. Komarneni, H. Katsuki, *Chem. Commun.* **2000**, 2389; b) C. S. Cundy, R. J. Plaisted, J. P. Zhao, *Chem. Commun.* **1998**, 1465; c) S. Mintova, S. Mo, T. Bein, *Chem. Mater.* **1998**, *10*, 4030; d) P. Chu, F. G. Dwyer, Patent US 4778666, **1988**; e) D. S. Kim, J.-S. Chang, J. S. Hwang, S.-E. Park, J. M. Kim, *Microporous Mesoporous Mater.* **2004**, *68*, 77.
[13] a) S. H. Jhung, J.-S. Chang, S.-E. Park, P. M. Forster, G. Férey, A. K. Cheetham, *Chem. Mater.* **2004**, *16*, 1394; b) M. Ganschow, G. Schulz-Eldoff, M. Mark, M. Wendschuh-Josties, D. Wöhrle, *J. Mater. Chem.* **2001**, *11*, 1823.
[14] E. Duprey, P. Beaunier, M.-A. Springuel-Huet, F. Bozon-Verduraz, J.-M. Manoli, J.-M. Bregeault, *J. Catal.* **1997**, *165*, 22.
[15] A. L. Allred, E. G. Rochow, *J. Inorg. Nucl. Chem.* **1958**, *5*, 264.
[16] P. W. Atkins, *Physical Chemistry*, 6th ed., Oxford University Press, Oxford, **1999**, p. 651.
[17] a) M. Ogura, S.-I. Nakata, E. Kikuchi, M. Matsukata, *J. Catal.* **2001**, *199*, 41; b) S. Klein, W. F. Maier, *Angew. Chem.* **1996**, *108*, 2376; *Angew. Chem. Int. Ed. Engl.* **1996**, *35*, 2230.
[18] a) P. Szabelski, J. Narkiewicz-Michalek, W. Rudziński, *Appl. Surf. Sci.* **2002**, *196*, 191; b) S. Nair, M. Tsapatsis, *J. Phys. Chem.* B **2000**, *104*, 8982; c) S. Mohanty, H. T. Davis, A. V. McCormick, *Chem. Eng. Sci.* **2000**, *55*, 2779; d) P. Szabelski, J. Narkiewicz-Michalk, *Langmuir* **2001**, *17*, 61.

